ELSEVIER

Dyes and Pigments 42 (1999) 159–172

DYES and PIGMENTS

Effects of fluorination on the properties of organic pigments

Greig Chisholm [a,*], Barry Hay [a], Kenneth D.M. Harris [b], Simon J. Kitchin [b], Keith M. Morgan [c]

[a] *Ciba Specialty Chemicals plc, Hawkhead Road, Paisley, PA2 7BG, UK*
[b] *School of Chemistry, University of Birmingham, Edgbaston, Birmingham B15 2TT, UK*
[c] *School of Textiles, Heriot Watt University, Netherdale, Galashiels, TD1 3HF, Scotland, UK*

Received 1 December 1998; accepted 18 December 1998

Abstract

The solid state properties of two fluorinated pigments are compared with their unfluorinated analogues and the influence of fluoro substitution upon the solid state properties is discussed. The effect of fluorination was examined by a range of techniques including UV/visible spectroscopy, solid state NMR spectroscopy and powder X-ray diffraction. Fluorination modified the crystal packing of the molecules and subsequently altered the pigmentary performance of the compounds. In both cases fluorination gave rise to compounds with poorer fastness properties. © 1999 Elsevier Science Ltd. All rights reserved.

Keywords: Solid state NMR; Pigment; Fluorination; Crystal

1. Introduction

A patent disclosing the properties of the trifluoromethylated organic pigment **1** for use in the colouration of polymer matrices has been filed recently [1]. This patent claims improved heat stability over similar non-fluorinated materials. Such heat stability is of great importance for organic pigments used in plastics, due to the severe processing conditions that are often employed in this industry. Clearly the pigment must not suffer any change in shade due to chemical degradation, polymorphic change or Ostwald ripening.

Fluorinated pigments are comparatively rare. The comprehensive review of organic pigments by Herbst and Hunger [2] mentions examples in only two pigment classes: (a) the benzimidazolone pigments, C.I. Yellow 154 (**2**) and C.I. Orange 60 (**3**), and (b) the disazo condensation pigments C.I. Yellow 128 (**4**) and C.I. Red 242 (**5**). All of these fluorinated pigments are reported to have excellent fastness properties, perhaps due to the additional potential for intermolecular hydrogen bonding with the presence of the fluorine substituents.

However, no systematic comparison between fluorinated organic pigments and the corresponding non-fluorinated pigments has been reported in the literature. In order to shed light on the effects of fluorination on the properties of pigments, two fluorinated pigments and their non-fluorinated analogues have been studied in the present work. Compounds **6** and **7** are based on the common monoazoanilide pigments, and are characterized

* Corresponding author. Tel.: +44-0141-887-1144; fax: +44-0141-840-2283.

0143-7208/99/$ - see front matter
PII: S0143-7208(98)00091-6

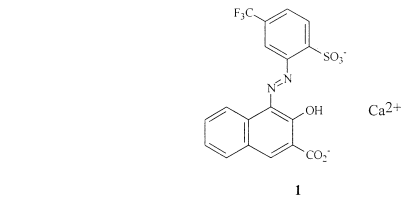

1

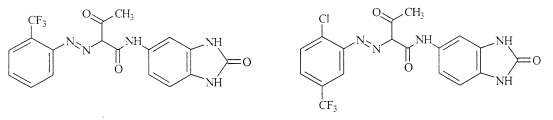

2 3

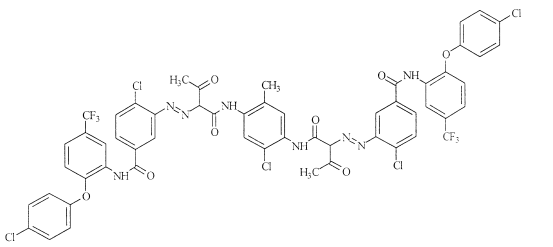

4

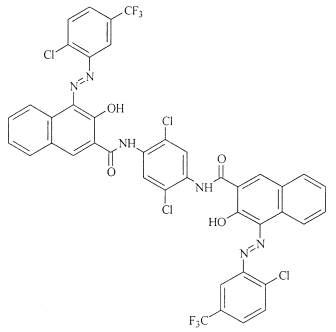

5

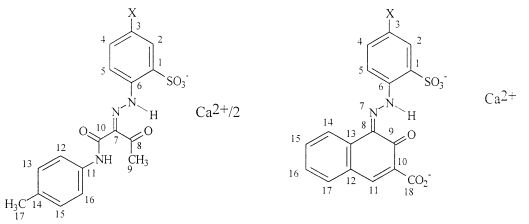

6, X = H
7, X = F
8, X = H
9, X = F

by their strong yellow hue. Compounds **8** and **9** are structurally similar to the monoazo red toner pigments. Although characterised as azo pigments, most pigments of this class actually exist as the keto-hydrazone tautomer (Fig. 1).

The crystal structure of an organic pigment is critical in determining properties such as the hue and the stability to solvent, heat and light. Furthermore, the colour strength, hiding power, stability, flow and dispersion properties of a pigment material [3] depend on the crystal morphology and the nature of the major surfaces of the crystal, and these properties again depend on the crystal structure. From all these aspects, the crystal structure is critically important in determining the properties of the pigment. Thus, it is clear that differences in the pigmentary properties of fluorinated and non-fluorinated materials may originate from differences in the structural properties of these materials.

It is well known [4] that replacement of hydrogen by fluorine can cause profound changes in the biological activity of organic molecules. The steric demands of fluorine are similar to those of hydrogen (Van der Waals radii 1.35 Å and 1.20 Å, respectively), so changes in conformational recognition are not expected. However, the special electronic character of fluorine can give rise to pronounced neighbouring group effects and allows the fluorine to act as a hydrogen bond acceptor. The C–F bond is very robust and is thought to impart increased lipophilicity, which is important in terms of bioavailability. Of particular interest to the study of organic pigments is the possibility of the fluorine acting as a hydrogen bond acceptor. Previous work on crystal engineering using fluorine [5,6] has suggested that changes in crystal packing associated with the presence of fluorine can be due

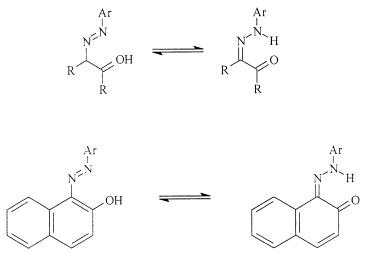

Fig. 1. Keto-hydrazone tautomerism.

to strong intermolecular interactions involving fluorine, although for non-planar molecules, details of the molecular geometry and conformation may be a more important consideration.

The effect of fluorination on the solid state and colouristic properties of the selected pigments are presented below. In principle, fluorination may manifest itself in a number of ways with regard to the structural properties of the solid. For the materials of interest here, the crystal structures are not known, due in part to the difficulty of preparing single crystals appropriate for conventional single crystal X-ray diffraction studies. Under these circumstances, a variety of alternative approaches are required to establish different aspects of the structural properties of these materials.

2. Results and discussion

Compounds **6–9** were prepared using standard azo coupling procedures (see Scheme 1 and Experimental). Both solution state ^{1}H and ^{13}C NMR spectra provide evidence for the keto-hydrazone tautomer in solution. In the ^{1}H NMR spectrum of the non-fluorinated pigment **6**, a broad singlet at 14.3 ppm was attributed to the hydrazo hydrogen. The ^{13}C NMR spectrum has the appropriate number of quaternary carbons, as assigned by a DEPT spectrum, to account for the keto-hydrazo tautomer. Similarly the fluorinated pigment **7** has a broad singlet at 14.4 ppm in the ^{1}H NMR spectrum and the appropriate number of quaternary carbon resonances in the ^{13}C NMR spectrum. For pigments **8** and **9**, ^{1}H NMR spectra are too broad to be diagnostic, but the ^{13}C NMR spectra show ketone resonances at 175.3 ppm for **8** and 174.3 ppm for **9**.

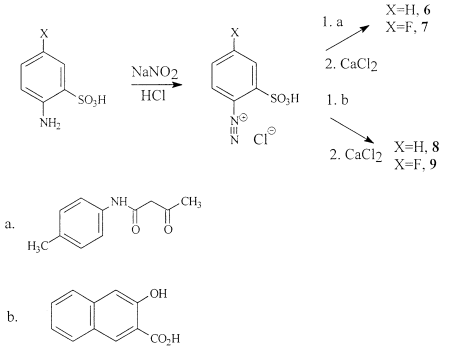

Scheme 1.

The UV/visible absorption spectra of the anilide pigments **6** and **7** in DMSO solution are almost identical. Equally, the UV/visible absorption spectra for the naphthol pigments **8** and **9** in DMSO solution are also almost identical. Thus, fluorination of the aromatic ring has little effect on the electronic properties of the molecules in solution. This was not the case for UV/visible absorption spectra recorded in the solid state, for which both fluorinated compounds **7** and **9** exhibit significant bathochromic shifts in comparison with the corresponding non-fluorinated compounds **6** and **8**. The values of λ_{max} for each compound are shown in Table 1. The observed differences in the solid state UV/visible absorption spectra for the fluorinated and non-fluorinated compounds illustrate the influence of crystal packing and the associated intermolecular and intramolecular interactions on the electronic properties of these solids.

Clearly, to understand the effects of fluorination on the properties of the pigments requires knowledge of the crystal structures of these materials. In general, introducing an additional functional group in a molecule may influence the crystal packing in a number of ways. For example: (a) it may force the molecular conformation to be altered; (b) it may give rise to a substantial change in the electronic structure of the molecule which in turn may give rise to alternative preferred modes of aggregation in the solid based on electrostatic interactions; (c) it may create the possibility for specific new types of intermolecular interactions (such as hydrogen bonding).

Table 1
λ_{max} for pigments **6–9** in solution state and solid state UV/visible absorption spectra

Compound	λ_{max}/nm solution	λ_{max}/nm solid state	$\Delta\lambda_{max}$/nm (solid state–solution)
6	375	375	0
7	375	387	12
8	510	556	46
9	511	561	50

In principle, any (or all) of these factors may be influential on introducing a fluorine substituent to a molecule. In the present case, however, factor (a) is not likely to be important, as the fluorine substituent is unlikely to disrupt the preference for a planar geometry of these molecules. Indeed, energy minimization calculations (carried out on the isolated molecules using the Cerius^{2TM} package [7] with the Dreiding force field (which has previously proven useful in describing the properties of organic pigments [8]) suggest that the molecular geometry and conformation is essentially identical for pigments **6** and **7** and essentially identical for pigments **8** and **9**. These predicted similarities in the molecular geometries and conformations of these pairs of pigments are supported by the results of UV/visible absorption spectra recorded in solution (see discussion above, and Table 1).

In common with most pigments, the materials studied here were isolated as fine powders, and were compared by powder X-ray diffraction [Fig. 2(a)–(d)]. In each case, the fluorinated and non-fluorinated pigments are not isostructural. For pigments **6** and **7**, the differences in the powder diffraction patterns are substantial. For pigments **8** and **9**, there is, perhaps, a greater degree of similarity in the positions of peaks in the powder diffraction patterns (suggesting that these materials may be based on unit cells with certain common features), although it is again clear from a qualitative comparison that these materials are not isostructural. In both cases, the fluorinated material is apparently less crystalline than the non-fluorinated material. Thus, the powder diffraction patterns for both fluorinated materials **7** and **9** show evidence for a significant amorphous component, and the peaks in both cases are significantly broader than for the non-fluorinated analogues **6** and **8**. It was not possible to grow single crystals of sufficient size to carry out conventional single crystal X-ray diffraction experiments for any of the materials **6–9**, and at present the actual structures of these materials remain unknown. The best opportunity for determination of the crystal structures of these pigments is from powder diffraction data [9–11], and future experiments in this direction are planned.

In the absence of knowledge of the crystal structures from diffraction studies, a series of high-resolution solid state ^{13}C NMR and ^{19}F NMR experiments have been carried out to assess structural aspects of these materials. The ^{13}C NMR results have proved to be more informative and are now discussed in detail. We recall that a high-resolution solid state ^{13}C NMR spectrum should, in principle, contain one peak for each crystallographically distinguishable ^{13}C environment in the structure. The isotropic chemical shift depends both on the molecular structure and conformation, *and* on the intermolecular environment in the solid. Knowledge of chemical shifts for the same molecule in solution, or from calculations for the isolated molecule, provide a reasonable first approximation to the isotropic chemical shift in the solid (provided the molecular conformations are similar). Effects due to the intermolecular environment in the solid give rise to further second order displacements in the isotropic chemical shift. Unless some very specific interactions are involved, the observed isotropic chemical shift for the solid typically differs by not more than about ± 5 ppm from the chemical shift of the isolated molecule or in solution.

For all pigments **6–9**, the ^{13}C NMR spectra show a large number of peaks in the approximate range 120–140 ppm, mainly due to the large number of aromatic ^{13}C environments in the molecule. Only peaks lying outside this range may be assigned confidently and are therefore useful for diagnostic purposes.

For pigment **6**, the ^{13}C NMR spectrum [Fig. 3(a), Table 2] is consistent with the molecule existing in the keto form in the solid state. In addition to the assignment for the carbonyl environment C8 as the keto form, the absence of any peak in the window between about 139 ppm and 161 ppm suggests that the enol form is not present (the peak due to C6 in the enol form is expected at ca. 147 ppm). The peak due to C10 contains a prominent shoulder, probably arising from ^{13}C–^{14}N residual dipolar interaction [12]. Interestingly, a pair of peaks are observed for both the carbonyl carbon (C8) and the methyl carbon (C9) of the acetyl group ($-COCH_3$), and are consistent with disorder of this group between two orientations

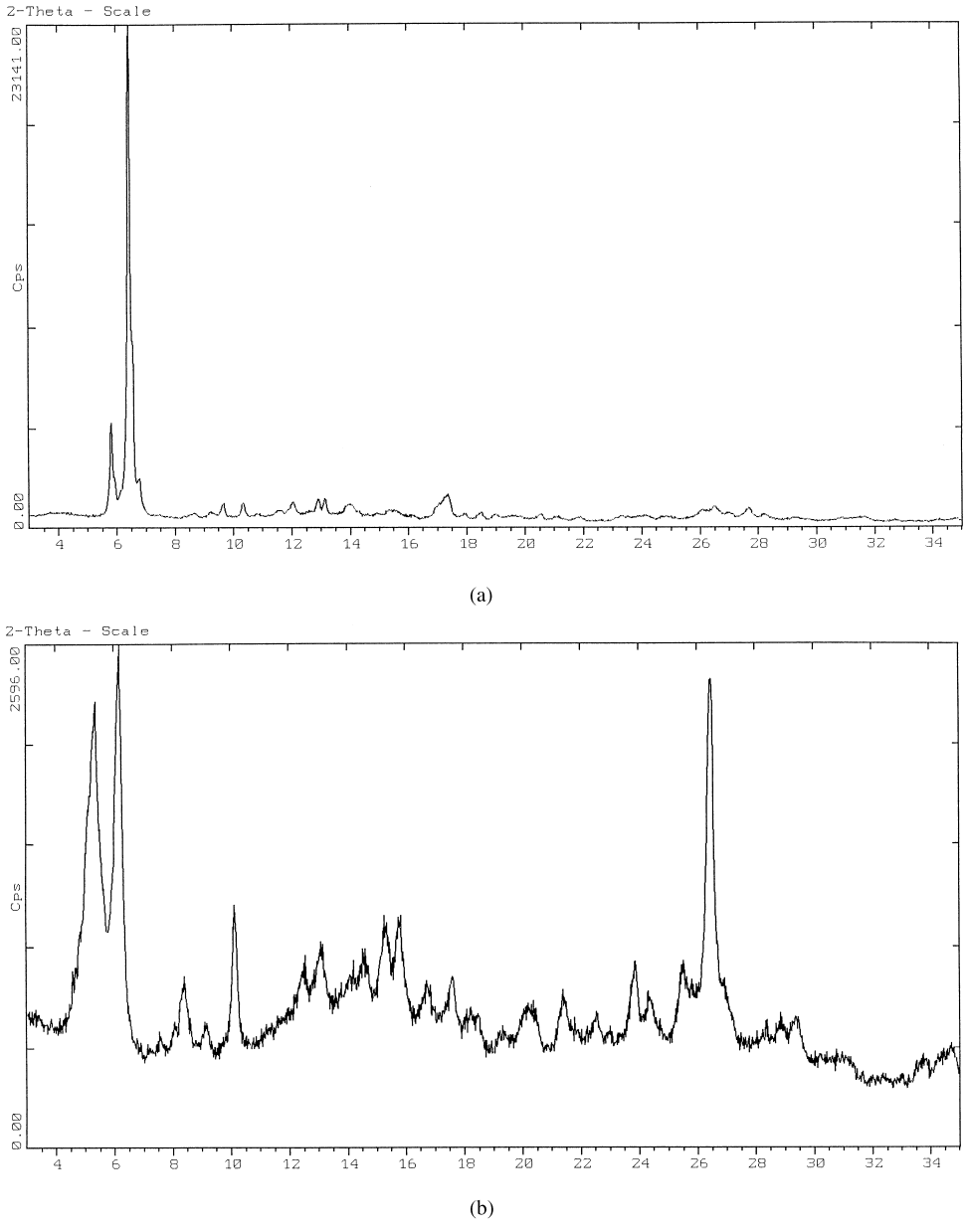

Fig. 2. Powder X-ray diffraction patterns of (a) pigment **6**; (b) pigment **7**; (c) pigment **8**; and (d) pigment **9**.

(related by 180° rotation about the C8–C7 bond). These two orientations of the acetyl group should correspond to two alternative modes of intramolecular hydrogen bonding involving the oxygen atom of this group. For the corresponding fluorinated material, pigment **7**, the ^{13}C NMR spectrum [Fig. 3(b), Table 2] is again consistent with the molecule existing in the keto form in the solid

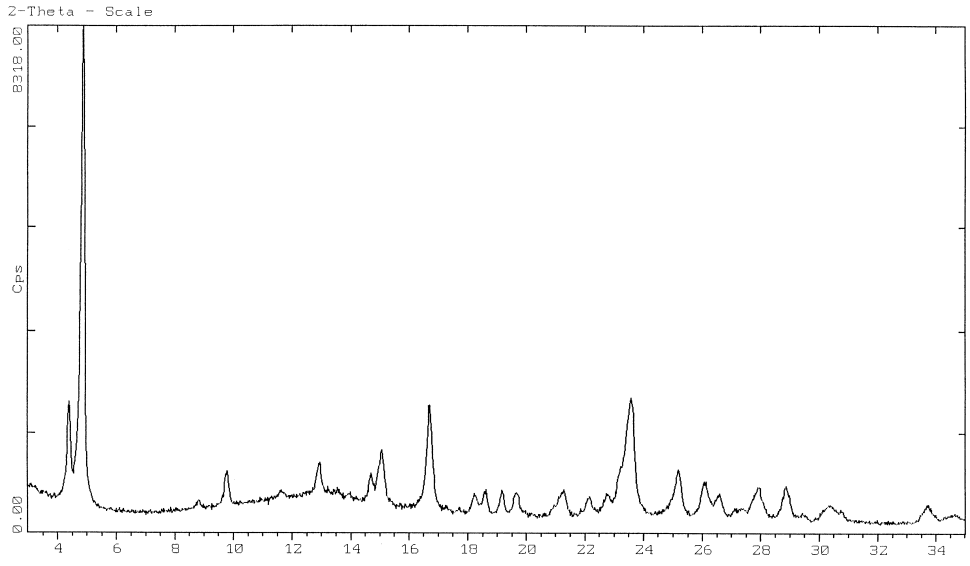

(c)

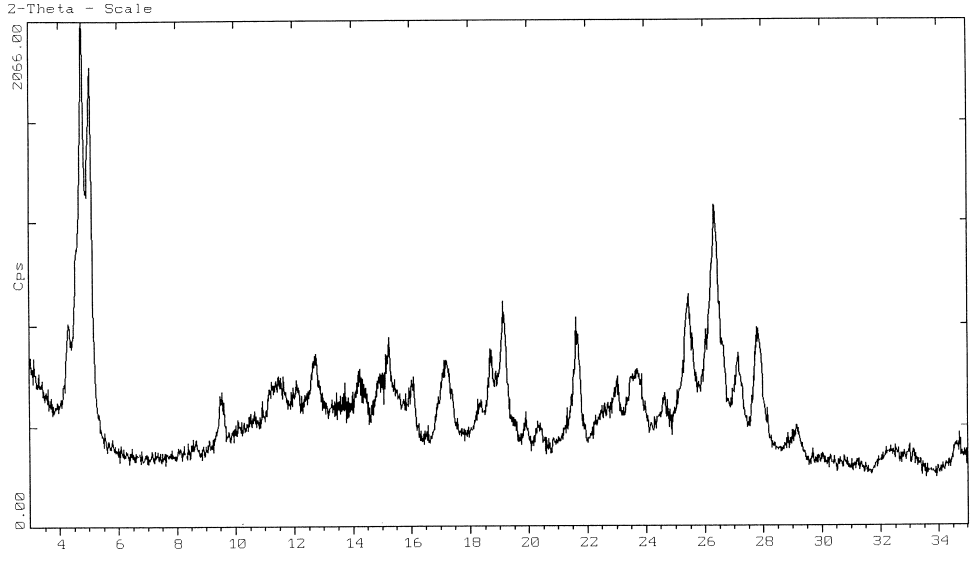

(d)

Fig. 2. *cont.*

state. Again, in addition to the assignment of the carbonyl environment C8 as the keto form, the absence of any peak in the window between about 136 ppm and 156 ppm due to C6 suggests that the enol form is not present. Interestingly, there is no evidence for disorder of the acetyl group between two orientations in this case. The peak due to the carbon (C3) bonded to fluorine is observed, although overlapped with the peak due to C10. Both of these peaks are expected to be broad, due

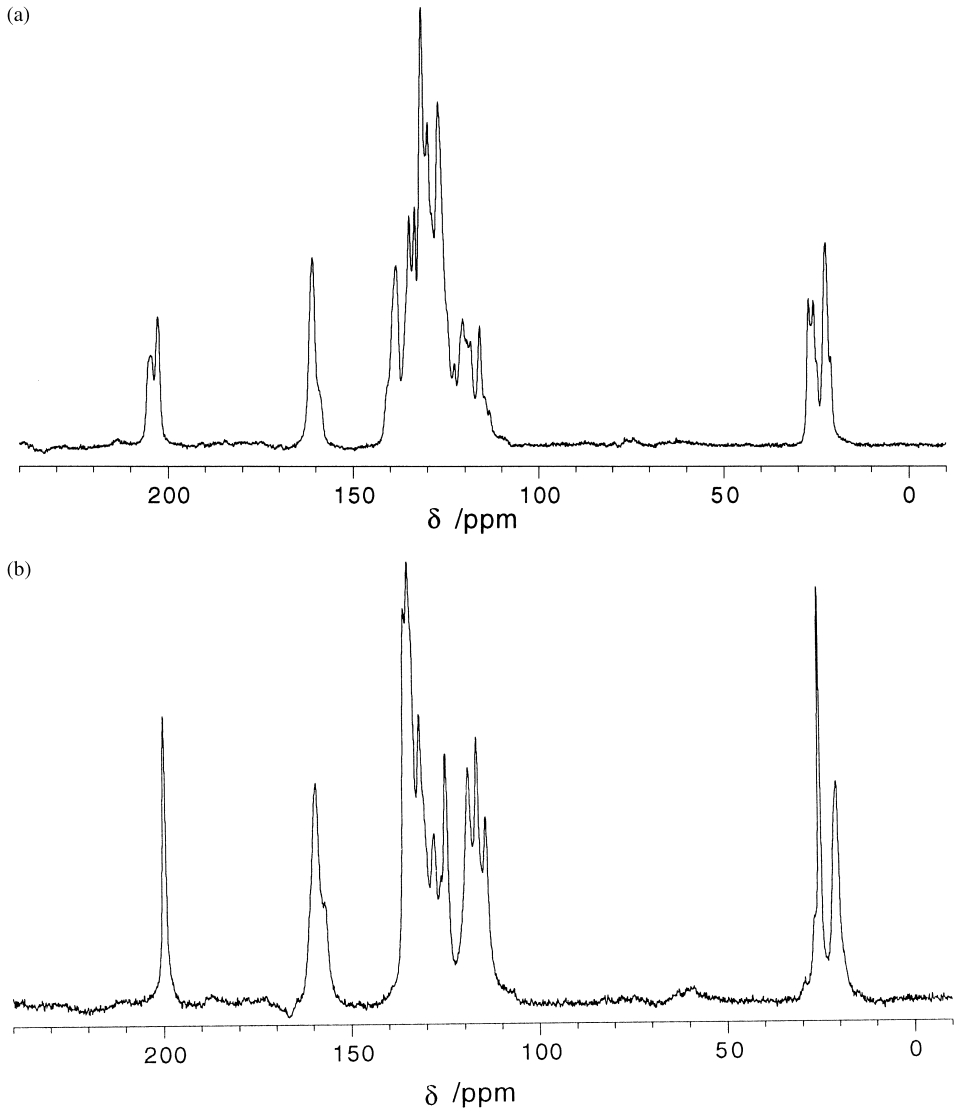

Fig. 3. (a) High-resolution solid state ^{13}C NMR spectrum for pigment **6**; (b) high-resolution solid state ^{13}C NMR spectrum for pigment **7**.

to ^{13}C–^{14}N residual dipolar interaction [12] in the case of C10 and ^{13}C–^{19}F dipolar coupling in the case of C3 [note: (a) ^{19}F decoupling was not used in recording the spectrum, although magic angle sample spinning substantially averages the direct dipolar interaction; (b) no J-coupling is resolved—if present, it is obscured by overlap with the peak representing C10]. Although qualitative comparison of the ^{13}C NMR spectra of pigments **6** and **7** suggests that there are significant structural differences between these materials, we cannot establish the details of the structural differences on the basis of this evidence alone. The high-resolution solid state ^{19}F NMR spectrum of pigment **7** [Fig. 4(a)] shows a single peak, verifying that there is one molecule in the asymmetric unit (consistent with observations from ^{13}C NMR). The isotropic chemical shift is consistent with that expected for this

Table 2
Diagnostic peaks in high-resolution solid state ^{13}C NMR spectra of pigments **6–9**. Assignments refer to the atom numbering scheme used in the definition of the molecular structures. Predicted chemical shifts were obtained from the program SpecInfo 3.1.6 [13] and are calculated for the isolated molecule in the keto or enol forms (and thus take no account of intermolecular effects that may influence the isotropic chemical shifts for solids). For entries marked**, see the discussion in the text

Compound	δ/ppm experimental	δ/ppm predicted (keto form)	δ/ppm predicted (enol form)	Assignment
6	202.9, 204.9	198.6	190.2	8
	161.1	162.9	164.8	10
	**	137.1	147.4	6
	25.9, 27.2	25.8	24.7	9
	22.7	21.8	21.8	17
7	199.7	198.6	190.2	8
	156.9 or 159.1	162.9	164.8	10
	156.9 or 159.1	157.4	157.4	3
	**	137.1	147.4	6
	25.1	25.8	24.7	9
	20.6	21.8	21.8	17
8	179.3	174.2	171.3	18
	171.0	172.1	155.4	9
9	173.9 or 175.1	174.2	171.3	18
	173.9 or 175.1	172.1	155.4	9
	159.0	157.4	157.4	3

type of molecule, and cannot be used alone to derive detailed information on the intermolecular environment around the fluorine atom.

For pigment **8**, the ^{13}C NMR spectrum [Fig. 5(a), Table 2] is consistent with the molecule existing in the keto form in the solid state (the isotropic chemical shift for C9 provides unambiguous evidence for this assignment). For the corresponding fluorinated material, pigment **9**, the ^{13}C NMR spectrum [Fig. 5(b), Table 2] is again consistent with the molecule existing in the keto form in the solid state (again, the isotropic chemical shift for C9 provides unambiguous evidence for this assignment). The peak due to the carbon (C3) bonded to fluorine is directly observed (although we note that no J-coupling is evident in this case). Although qualitative comparison of the ^{13}C NMR spectra of pigments **8** and **9** suggests that there are significant structural differences between these materials, we cannot establish the details of the structural differences on the basis of this evidence alone. The peaks in the ^{13}C NMR spectrum for pigment **9** are noticeably broader than those for pigment **8**, suggesting that pigment **9** may have a lower degree of crystallinity. This observation is consistent with our powder X-ray diffraction and transmission electron microscopy data for these materials. The high-resolution solid state ^{19}F NMR spectrum of pigment **9** [Fig. 4(b)] shows a single peak, verifying that there is one molecule in the asymmetric unit (consistent with observations from ^{13}C NMR). The isotropic chemical shift is consistent with that expected for this type of molecule, and cannot be used alone to derive detailed information on the intermolecular environment around the fluorine atom. Both the ^{13}C NMR and ^{19}F NMR spectra for pigment **9** contain a subset of peaks of very low intensity that have not been assigned, and probably originate from a small amount of an impurity phase.

Morphological differences between the fluorinated and non-fluorinated pigments have been studied by transmission electron microscopy at $\times$60,000 magnification [Fig. 6(a)–(d)]. Pigment **6** has a thick rod morphology, whereas pigment **7** exists as long, thin rods. Pigment **8** gives rises to rod-like crystals with some plate character evident. Compound **9** forms a mixture of rods and plates. In all cases the fluorinated pigments give significantly smaller crystals, in particular compound **9**. This is consistent with our observations from powder X-ray diffraction and high-resolution solid state ^{13}C NMR, which suggest that the overall crystallinity of pigment **9** is poorer than pigment **8**. The dominance of a rod morphology is not surprising given the expected high growth rate in the $\pi - \pi$ direction.

As noted above, fluorinated pigments often exhibit superior fastness and stability properties in comparison with the corresponding non-fluorinated pigments. The light fastness and thermal behaviour of pigments **6–9** have been studied here. To test the light fastness, each pigment was dispersed into a PVC hide and exposed to a xenon arc lamp for 30 h. The light fastness for each pigment, obtained according to the blue-wool scale, is given in Table 3. Higher numbers indicate better light fastness. For these pigments, fluorination clearly

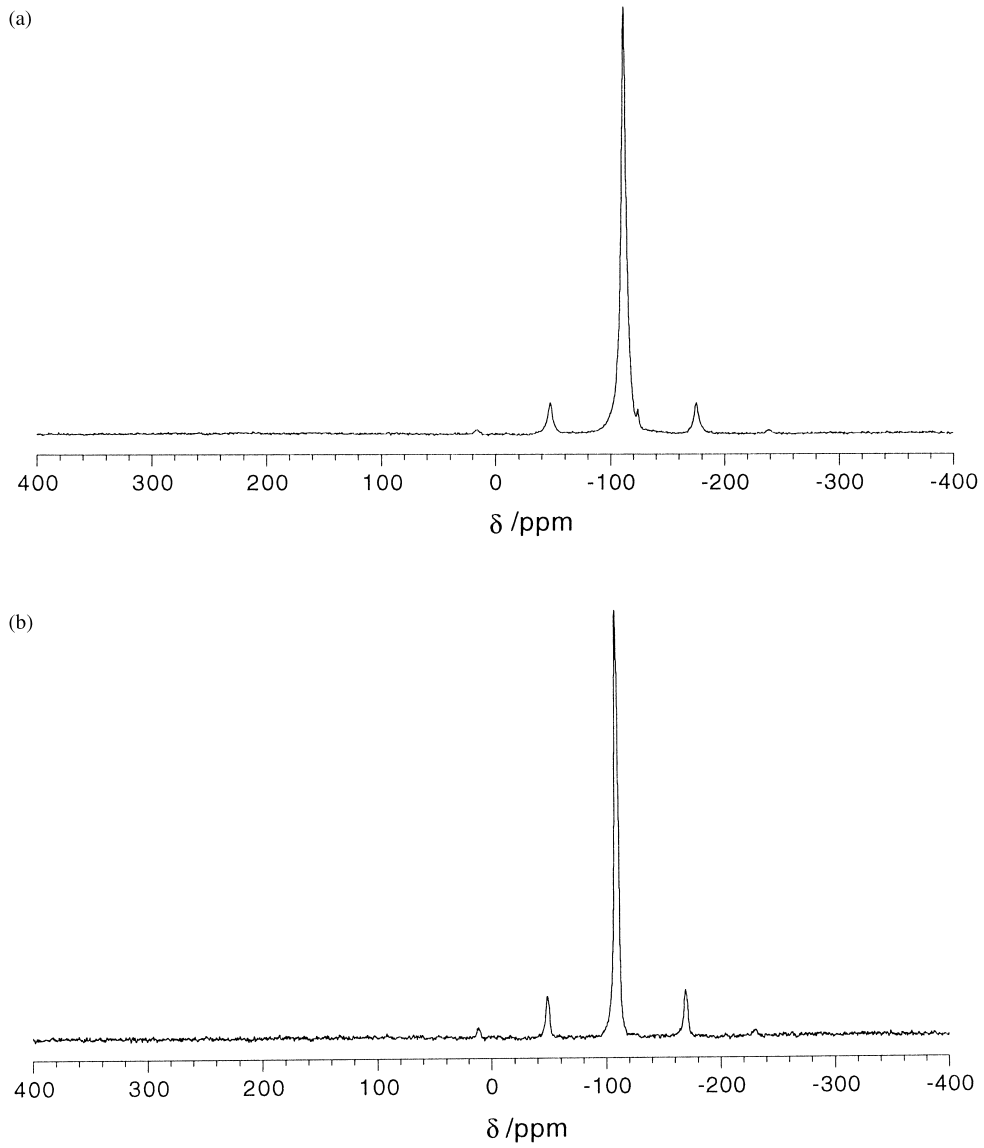

Fig. 4. (a) High-resolution solid state ^{19}F NMR spectrum for pigment **7**; (b) high-resolution solid state ^{19}F NMR spectrum for pigment **9**.

gives rise to poorer light stability, in contradiction with what is observed in the literature [1,2]. However, this observation further underlines the significant differences in properties that can be induced by fluorination.

A measure of light fastness alone is not enough to classify a material as "less stable", as light fastness may be determined not only by the molecular and crystal structure but also by the morphology of the crystal [3]. The thermal stability of pigments **6**–**9** was assessed by thermogravimetric analysis, revealing important differences in behaviour. Thus, as shown in Table 4, the temperature at which each fluorinated pigment begins to

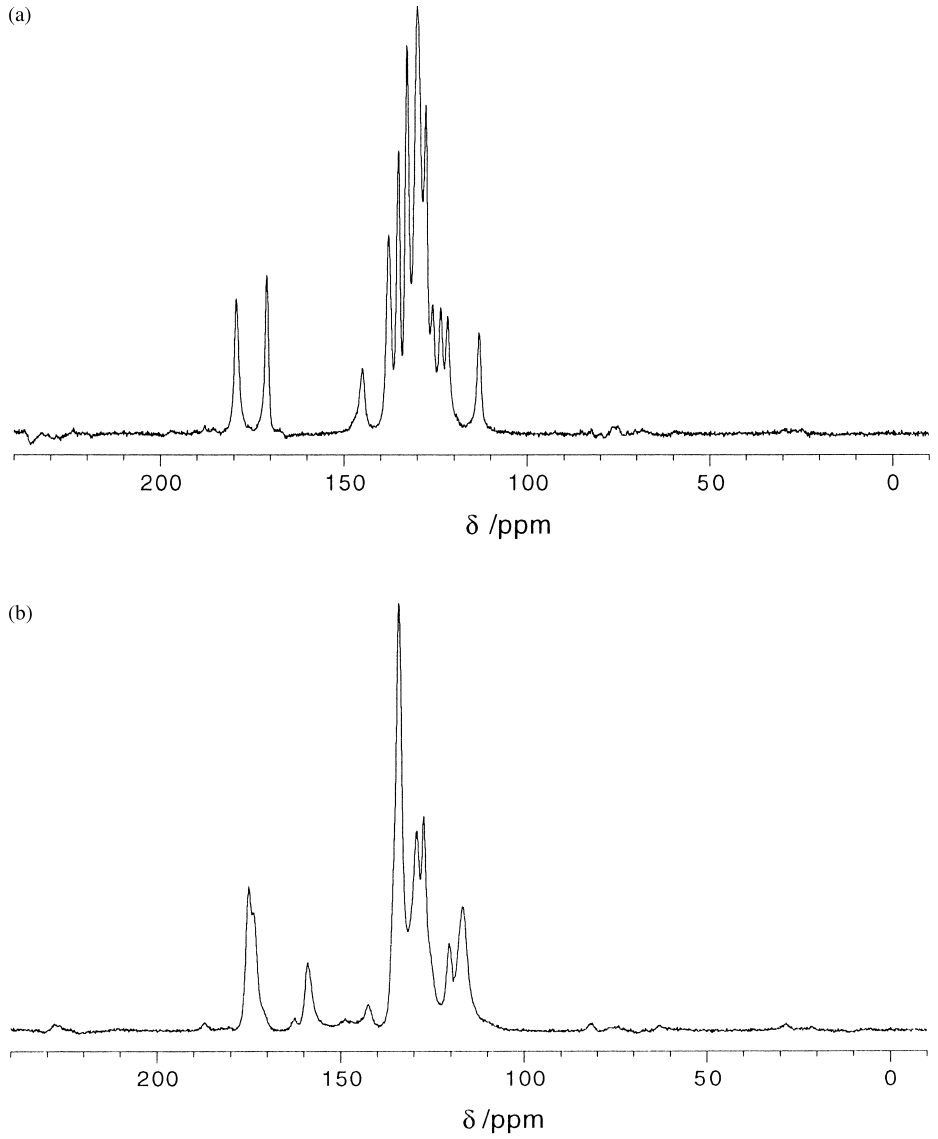

Fig. 5. (a) High-resolution solid state ^{13}C NMR spectrum for pigment **8**; (b) high-resolution solid state ^{13}C NMR spectrum for pigment **9**.

decompose is about 15°C lower than that for the corresponding non-fluorinated pigment.

3. Conclusions

Fluorine can exert a profound influence on the crystal packing of organic pigments, and can consequently influence the morphology and pigmentary performance. The effect of these changes on the application properties of the pigment are generally unpredictable and can result in pigments with poorer light fastness and thermal stability as shown in this paper, or may give rise to pigments with improved properties as disclosed previously in the pigment literature [1]. Our solid state NMR

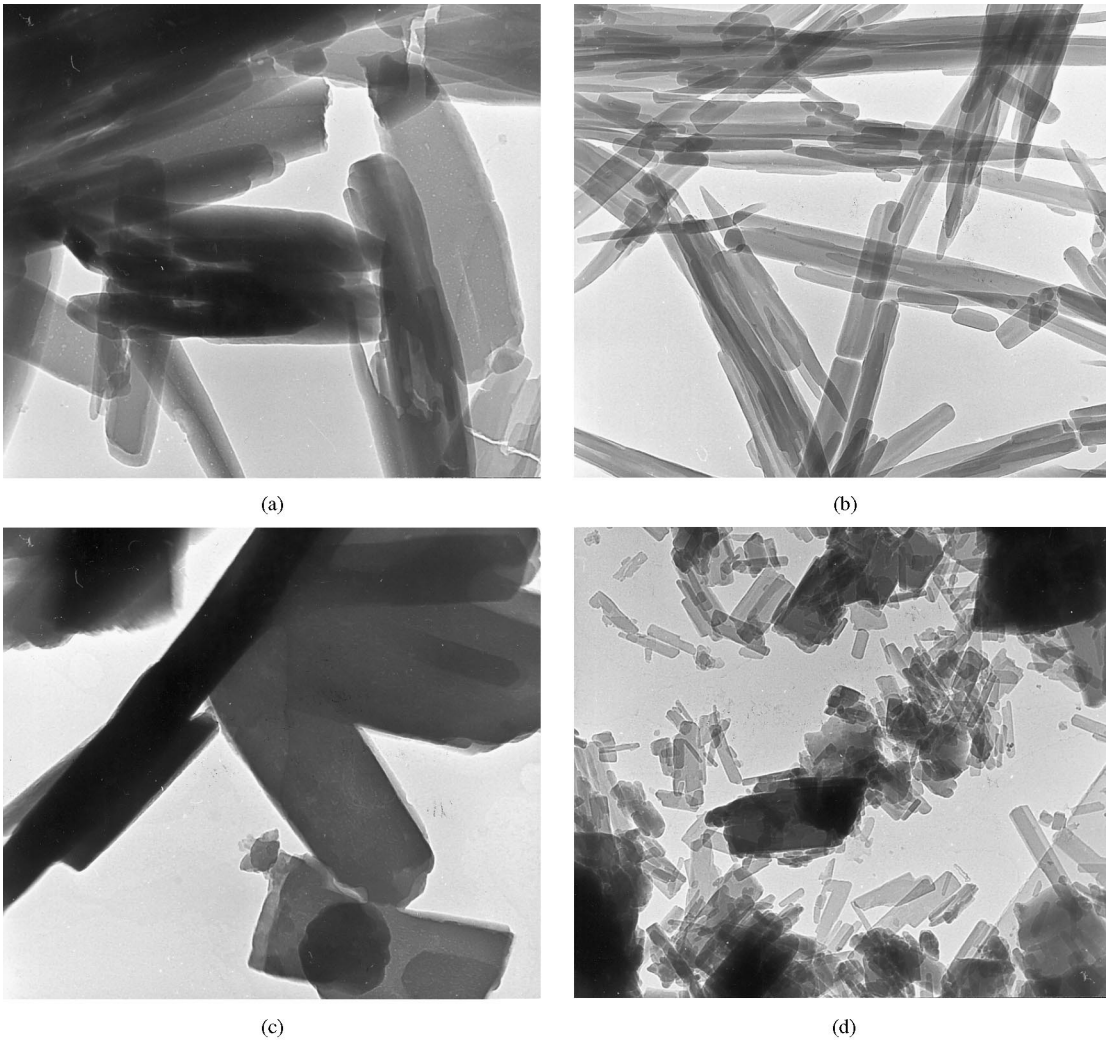

Fig. 6. Transmission electron micrographs of (a) pigment **6**; (b) pigment **7**; (c) pigment **8**; and (d) pigment **9**, showing their crystal morphologies.

studies have provided valuable insights into certain structural aspects of these materials, although they cannot yield detailed information on the differences in structure between the fluorinated and non-fluorinated pigments. Further work to determine the crystal structures of these pigments from powder diffraction data will provide a clearer understanding of the detailed relationships between crystal structure and pigment properties.

4. Experimental

4.1. Techniques

IR spectra were recorded on a Philips PU9800 spectrometer and UV/visible spectra were recorded on a Perkin Elmer Lambda 2 spectrometer. Solid state UV/visible spectra were recorded for thin films printed on a transparent substrate.

Table 3
Light fastness of pigments **6–9**

Compound	Light fastness
6	4
7	1
8	5
9	1

Table 4
Onset temperatures for decomposition of pigments **6–9** determined by TGA

Compound	T/°C
6	325
7	307
8	410
9	394

Solution state ^{1}H and ^{13}C NMR spectra were recorded on Bruker AC200 and Bruker DPX400 spectrometers, and chemical shifts are quoted relative to tetramethylsilane. Thermogravimetric analysis was carried out using a Metler Toledo TG-50 Thermobalance at a heating rate of 25°C/min. Powder X-ray diffraction patterns were recorded on a Siemens D5000 X-ray diffractometer in reflection mode using filtered CuK_{α} radiation. The total range of 2θ was 3°–35° measured in 0.02° steps and collected over 27 min. Transmission electron micrographs were recorded using a Philips EM300 instrument at operating voltage 100 kV. The instrumental magnification was 12,000 and the photographic magnification was 5.

Solid state ^{13}C NMR and ^{19}F NMR spectra were recorded on a Chemagnetics CMX-Infinity 300 spectrometer at 75.4 MHz (^{13}C) and 282.5 MHz (^{19}F). High-resolution solid state ^{13}C NMR spectra were recorded using $^{13}C^{1}H$ cross-polarisation, magic angle sample spinning and high-power ^{1}H decoupling. A Chemagnetics 9.5 mm probe was used, with spinning frequency (4000 ± 2) kHz and ^{1}H decoupler field strength ca. 40 kHz. All spectra were recorded using the TOSS sequence for sideband supression, and the TPPM decoupling sequence [14] (with 170° decoupling pulses and a 15° phase) spectra were recorded for all samples using the dipolar dephasing technique to assist in spectral assignment. Chemical shifts are reported relative to tetramethylsilane. High-resolution solid state ^{19}F NMR spectra were recorded using magic angle sample spinning and high-power ^{1}H decoupling. A Chemagnetics 4 mm H/F probe was used, with spinning frequency (17,000 ± 5) Hz or (18,000 ± 5) Hz and ^{1}H decoupler field strength ca. 50 kHz. Chemical shifts are reported relative to $CFCl_3$.

*4.2. Synthesis and characterization of the calcium salt of 2-[(2-sulfophenyl)azo]-*N*-(4-methylphenyl)-3-oxo-butanamide* (**6**)

2-Amino-benzenesulphonic acid (13.7 g, 0.08 mol) was dissolved in a mixture of water (100 ml) and 47% aqueous sodium hydroxide solution (7.1 g, 0.08 mol). The solution thus obtained was cooled to 0°C by addition of ice. A solution of sodium nitrite (5.5 g, 0.08 mol) in water (25 ml) was prepared. The bulk of this solution was added to the amine solution, followed by HCl (22.0 g 0.22 mol at 36%). The remainder of the sodium nitrite solution was added over 45 min to give the diazonium salt of the amine.

In a separate vessel, acetoacet-*p*-toluidide (15.7 g, 0.08 mol) was dissolved in a mixture of 47% aqueous sodium hydroxide solution (24.2 g, 0.08 mol) and water (300 ml). Glacial acetic acid (9.5 g) was added dropwise over 5 min to give a slurry of the anilide. This slurry was cooled to 8°C by addition of ice. The diazo solution was added over 50 min, followed by calcium chloride (16.6 g, 0.12 mol at 80%) to give the pigment slurry. The pH of the slurry was adjusted to 7.4 by addition of dilute sodium hydroxide solution. The slurry was then heated to 95°C via steam injection and maintained at this temperature for 30 min. The slurry was cooled to 70°C, filtered and washed salt free with water. The presscake obtained was dried at 70°C for 16 h to give the product (29.9 g, 95%). IR (KBr, $\bar{\nu}$/cm^{-1}) 1661 (ketone, C=O stretch), 1601 (amide I, C=O stretch), 1554 (amide II, N–H bend); ^{1}H NMR (d_6-DMSO, δ/ppm) 2.2 (3H, s, CH_3–Ar), 2.5 (3H, s, CH_3–C=O), 6.3–8.4 (8-H, m, aromatic H), 11.0 (1H, bs, amide H), 14.3 (1H, bs, hydrazo H); ^{13}C NMR (d_6-DMSO, δ/ppm) 21.0 ($\underline{C}H_3$–Ar), 26.5 ($\underline{C}H_3$–C=O), 116.0 (aromatic CH), 120.4 (aromatic CH2), 124.2 (aromatic CH), 127.8 (aromatic CH),

128.3 (C), 129.8 (aromatic CH2), 131.0 (aromatic CH), 133.7 (quaternary C), 135.3 (quaternary C), 135.4 (quaternary C), 139.0 (quaternary C), 160.9 (amide C=O), 199.3 (ketone C=O).

4.3. Synthesis and characterization of the calcium salt of 2-[(4-fluoro-2-sulfophenyl)azo]-N-(4-methyl-phenyl)-3-oxo-butanamide (**7**)

Compound **7** was synthesised in an identical manner to **6**, except that 2-amino-4-fluorobenzenesulfonic acid (15.3 g, 0.08 mol) was used as the amine. The product was obtained as a yellow powder (31.6 g, 96%). IR (KBr, $\bar{\nu}$/cm^{-1}) 1664 (ketone, C=O stretch), 1604 (amide I, C=O stretch), 1506 (amide II, N–H bend); ^{1}H NMR (d_6-DMSO, δ/ppm) 2.2 (3H, s, CH_3–Ar), 2.4 (3H, s, CH_3–C=O), 6.7–8.3 (7-H, m, aromatic H), 11.0 (^{1}H, bs, amide H), 14.4 (1H, bs, hydrazo H); ^{13}C NMR (d_6-DMSO, δ/ppm) 21.3 ($\underline{C}H_3$–Ar), 26.9 (CH3–C=O), 114.2 (aromatic CH, d, *J* 23 Hz), 124.2 (aromatic CH, d, *J* 24 Hz),120.6 (aromatic CH), 121.2 (2aromatic CH), 130.0 (aromatic C), 130.5 (2aromatic CH), 135.3 (quaternary C), 135.6 (quaternary C), 136.5 (quaternary C), 158.3 ($\underline{C}$–F, d, *J* 249 Hz), 161.1 (amide C=O), 199.5 (ketone C=O).

4.4. Synthesis and characterization of the calcium salt of 3-hydroxy-4-[(2-sulfophenyl)azo]-2-naphthalenecarboxylic acid (**8**)

2-Amino-benzenesulphonic acid (13.7 g, 0.08 mol) was dissolved in a mixture of water (100 ml) and 47% aqueous sodium hydroxide solution (7.1 g, 0.08 mol). The solution thus obtained was cooled to 0°C by addition of ice. A solution of sodium nitrite (5.5 g, 0.08 mol) in water (25 ml) was prepared. The bulk of this solution was added to the amine solution, followed by HCl (22.0 g, 0.22 mol at 36%). The remainder of the sodium nitrite solution was added over 45 min to give the diazonium salt of the amine.

In a separate vessel, 2-hydroxy-3-naphthoic acid (18.8 g, 0.08 mol) was dissolved in a mixture of 47% aqueous sodium hydroxide solution (24.2 g, 0.08 mol) and water (300 ml) at 60°C. This slurry was cooled to 8°C by addition of ice. The diazo solution was added over 60 min. The slurry thus obtained was stirred for 2 h at 8–10°C prior to addition of calcium chloride (33.3 g, 0.24 mol at 80%) to give the pigment slurry. Stirring was continued for 1 h, with the temperature of the reaction mixture allowed to rise to ambient temperature. The pH of the slurry was adjusted to 7.4 by addition of dilute sodium hydroxide solution. The slurry was then heated to 95°C via steam injection and maintained at this temperature for 30 min. The slurry was cooled to 70°C, filtered and washed salt free with water. The presscake obtained was dried at 70°C for 16 h to give the product (31.8 g, 97%). IR (KBr, $\bar{\nu}$/cm^{-1}) 1623 (ketone, C=O stretch), 1605 (carboxylic acid, C=O stretch), 1569 (C=C stretch); ^{1}H NMR (d_6-DMSO, δ/ppm) 6.6–8.9 (bm, aromatic H); ^{13}C NMR (d_6-DMSO, δ/ppm) 117.8 (aromatic CH), 121.8 (aromatic CH), 123.9 (aromatic C), 126.1 (aromatic C), 127.0 (aromatic CH), 127.2 (aromatic CH), 128.0 (aromatic CH), 129.7 (aromatic C), 131.4 (aromatic CH), 131.7 (aromatic CH), 132.5 (aromatic CH), 135.3 (aromatic C), 137.0 (aromatic C), 138.8 (aromatic C), 147.8 (unsaturated CH), 165.6 (carboxylic acid C=O), 175.3 (ketone C=O).

4.5. Synthesis and characterization of the calcium salt of 3-hydroxy-4-[(4-fluoro-2-sulfophenyl)azo]-2-naphthalenecarboxylic acid (**9**)

Compound **9** was synthesised in an identical manner to **8**, except that 2-amino-4-fluorobenzenesulfonic acid (15.3 g, 0.08 mol) was used as the amine and gave the product as a red powder (32.5 g, 95%). IR (KBr, $\bar{\nu}$/cm^{-1}) 1622 (ketone, C=O stretch), 1604 (carboxylic acid, C=O stretch), 1551 (C=C stretch); ^{1}H NMR (d_6-DMSO, δ/ppm) 7.2–8.7 (bm, aromatic H); ^{13}C NMR (d_6-DMSO, 100 MHz, δ/ppm) 114.3 (aromatic CH, d *J* 25 Hz), 118.1 (aromatic CH, d, J 23 Hz), 120.0 (aromatic CH, d J 8 Hz), 121.8 (aromatic CH), 124.3 (aromatic C), 126.2 (aromatic C), 127.0 (aromatic CH), 129.7 (aromatic C), 131.5 (aromatic CH), 132.3 (aromatic CH), 135.2 (aromatic C), 135.6 (aromatic C), 139.3 (aromatic C), 147.1 (unsaturated CH), 160.1 (aromatic C-F, d, *J* 245 Hz), 165.5 (carboxylic acid C=O), 174.3 (ketone C=O).

References

[1] Fraser I, Wilson S. (Ciba Geigy). European Patent 767219 1998.
[2] Herbst W, Hunger K. Industrial organic pigments. Weinheim, VCH, 1993.
[3] Hao Z, Iqbal A. Chem Soc Rev 1997; 26: 203.
[4] Filler R, Kobayashi Y, Yagupolskii LM, editors. Organofluorine compounds in medicinal chemistry and biomedical applications. Amsterdam: Elsevier, 1993.
[5] Hopkin SE, Muir M, Theocharis CR. J Chem Soc Perkin Trans 2 1991; 1131.
[6] Kumar VA, Venkatesan K. J Chem Soc Perkin Trans 2 1993; 2429.
[7] Cerius$^{2®}$, Version 3.5, Molecular Simulations Inc., 1997.
[8] Erk P, Hetzenegger J, Bohm A. European Coating Journal 1997; 906.
[9] Harris KDM, Tremayne M. Chem Mater 1996;8:2554.
[10] Tremayne M, Kariuki BM, Harris KDM. Angew Chemie Int Ed Engl 1997;36:770.
[11] Harris KDM, Johnston RL, Kariuki BM. Acta Cryst 1998;A54:632.
[12] Harris RK, Olivieri AC. Prog Nucl Magn Reson Spectrosc 1992;24:435.
[13] SpecInfo 3.1.6, Chemical Concepts GmbH, Weinheim, Germany.